Oscillation of channel branching ratios and *g-u*-symmetry state mixing in the direct photodissociation of HD

Jie Wang [*] and Yuxiang Mo [†]

Department of Physics and State Key Laboratory of Low-Dimensional Quantum Physics, Tsinghua University, Beijing 100084, China

(Received 30 December 2019; revised manuscript received 13 March 2020; accepted 6 April 2020; published 11 May 2020)

For the direct photodissociation of HD in the second threshold, there are four open channels $H(2s) + D(1s)$, $H(2p) + D(1s)$, $D(2s) + H(1s)$, and $D(2p) + H(1s)$. We measured the channel branching ratios and found that the ratios oscillate with the wave vectors of the photofragments. However, the population ratios $[H(2s)]/[H(2s) + D(2s)]$ and $[H(2p)]/[H(2p) + D(2p)]$ are nearly constant ~0.6. The results can be explained by assuming that the photodissociation in the Franck-Condon region follows mechanisms similar to those of H_2 and D_2, i.e., the excitations are to the $3p\sigma B'\,^1\Sigma_u^+$ and $2p\sigma B\,^1\Sigma_u^+$ states that are interfered with due to the phase differences between the two states. For HD, near the dissociation limits, the *g-u* pair states that are valid in the Born-Oppenheimer approximation are mixed almost completely in the corrected adiabatic approximation. A diabatic approximation would thus predict that the ratios $[H(2s)]/[H(2s) + D(2s)]$ and $[H(2p)]/[H(2p) + D(2p)]$ are 0.5.

DOI: 10.1103/PhysRevA.101.053418

I. INTRODUCTION

The photodissociation dynamics of small molecules is important not only in the understanding of the electronic structure of molecules, but also in practical applications, such as interstellar chemistry [1–3]. The dissociation features are closely related to the potential energy curves (PECs) and the associated scattering wave functions [4,5]. With H_2 as the simplest molecule, its electronic spectra and dissociation dynamics have drawn a great deal of attention [6–14]. For the direct dissociation of H_2 and D_2 near the second dissociation threshold, Beswick and Glass-Maujean predicted that the channel branching ratios of $2s + 1s$ and $2p + 1s$ oscillate as a function of the wave vectors of the photofragments [11,12]. Recently, we experimentally verified this prediction in the case of D_2 [15].

For H_2, there are three bound *u*-symmetry states adiabatically correlated with the second dissociation limits, in which the $3p\sigma B'\,^1\Sigma_u^+$ state correlates with the $H(2s) + H(1s)$ channel and $2p\sigma B\,^1\Sigma_u^+$ and $2p\pi C\,^1\Pi_u$ correlate with $H(2p) + H(1s)$ (see Fig. 1) [10–14]. The direct photodissociation occurs mainly via the nuclear vibrational continua of the $3p\sigma B'\,^1\Sigma_u^+$ and $2p\sigma B\,^1\Sigma_u^+$ states; the former is the dominant process. Due to the vibronic interaction between the two states, each dissociation limit actually results from the two states. Therefore, the interference occurring between the two paths leads to the channel $H(2s) + H(1s)$ or $H(2p) + H(1s)$. The summations of signal intensities of the two channels are approximately constant, indicating that the phases of the two oscillations are just reversed. The channel branching ratios depend on both the amplitude and relative phase of the scattering wave functions [11,12,15]. The phase differences between the two states are approximately proportional to the wave vectors of the photofragments. By tuning the excitation energies, the wave vectors of the photofragments change, the channel branching ratios thus oscillate due to the phase differences.

There have been many experimental and theoretical studies about the fragment spin-orbit branching ratios in the photodissociation, which are found to be dependent on the fragment kinetic energies and the spin-orbit coupling strengths [16–18]. The relative phases between the dissociation wave functions are usually not discussed. The phase controlled channel branching ratios would provide insight into the vibronic couplings in chemical reactions.

The direct dissociation of the HD molecule provides an interesting example of the state couplings and their relative phases on the channel branching ratios [19–30]. In contrast to H_2 and D_2, there are four open channels $D(2s) + H(1s)$, $D(2p) + H(1s)$, $H(2s) + D(1s)$, and $H(2p) + D(1s)$ [19–25]. In the Born-Oppenheimer approximation [1], the PECs should be independent of isotopes, as are the channel branching ratios. However, because of the isotope effect, the dissociation limits split into two energy levels $D(2s, 2p) + H(1s)$ and $H(2s, 2p) + D(1s)$, with a space of $\sim 22\,\mathrm{cm}^{-1}$. The Born-Oppenheimer approximation is therefore not valid near the asymptotes. With a correction of the Born-Oppenheimer approximation, the mass effect can be taken into account in the calculation of PECs [19–22]. The channel branching ratios should thus be dependent on the isotopes. In the following, we call the PEC including the mass effect a corrected adiabatic PEC and the one without the mass effect is the Born-Oppenheimer PEC. Note that the Born-Oppenheimer method is an adiabatic approximation in principle [1]. Figures 1(a)

[*]Present address: National Innovation Institute of Defense Technology, Academy of Military Sciences PLA China, Beijing 100071, China.

[†]Corresponding author: ymo@mail.tsinghua.edu.cn

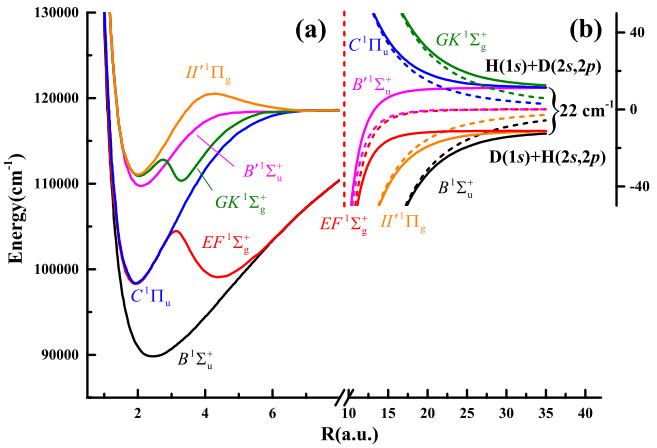

FIG. 1. Potential energy curves of the HD molecule adapted from Ref. [22]. (a) Born-Oppenheimer PECs. (b) The dotted lines are the Born-Oppenheimer PECs and the solid lines are the corrected adiabatic PECs that take account of the atomic masses. The Born-Oppenheimer PECs in the Franck-Condon region in (a) are similar to the corrected adiabatic PECs. Note that the threshold for the lower dissociation limit H($2s$) + D($1s$) is 118 664.8 cm^{-1} [10].

and 1(b) show the Born-Oppenheimer PECs and the corrected adiabatic PECs in the dissociation limits of the HD molecule, respectively.

For H_2 and D_2 molecules, the inversion of electronic wave functions in the center-of-mass coordinates is symmetric or antisymmetric and is referred to as a g or u symmetry, respectively. For HD, the g-u symmetry states are mixed in the corrected adiabatic PECs. Nevertheless, the g-u symmetries are approximately maintained in the Franck-Condon region. The photodissociation involves a change of dynamics from that described by the Born-Oppenheimer approximation in the Franck-Condon region to that described by the corrected adiabatic approximation near the dissociation limits. Because the photoexcitation is mainly due to the nuclear vibrational continua of the $3p\sigma B'\,^1\Sigma_u^+$ state [26–30], the main product channel would be D($2s$) + H($1s$) for the dissociation along the corrected adiabatic PEC. However, because of the nonadiabatic coupling near the dissociation limits, there should be a population transfer from the D($2s$) state to the H($2s$) state depending on the g-u state mixing. Therefore, the channel branching ratios in the photodissociation of HD should be dependent not only on the phase of the wave functions but also on the g-u state mixings.

Previously, there have been studies about the predissociation dynamics of HD [19–22,25,28]. Durup calculated the branching ratios between the H($2p$) + D($1s$) and D($2p$) + H($1s$) channels in the predissociation of HD and found that the former channel is more proportional [19]. Recently, we studied the predissociation of HD using an XUV laser pump and UV laser probe method and found large asymmetry between the H($2s$, $2p$) and D($2s$, $2p$) channels [25]. In this work we apply the same technique to study the direct dissociation of HD.

II. EXPERIMENTAL METHOD

The experimental setup consists of a tunable XUV laser pump (∼10 nJ/pulse), a UV laser probe system (365 nm and ∼1 mJ/pulse), and a typical velocity map imaging apparatus [15,25,31–35]. The XUV laser was generated by resonance enhanced four-wave sum mixing ($2\omega_1 + \omega_2$) in a pulsed Kr jet using two laser beams. The first laser beam with frequency ω_1 was generated by the tripling of a dye laser and $2\omega_1$ was equal to the resonance frequency of the transition $4p^5(^2P_{1/2})5p[1/2]_0 \leftarrow (4p^6)\,^1S_0$ (98 855.1 cm^{-1}) of the Kr atom. The second laser beam (ω_2) was tuned from 23 300 to 19 800 cm^{-1} or from 429 to 505 nm using five different laser dyes. The two dye lasers were pumped by an Nd:YAG laser (repetition rate 20 Hz). The two fundamental beams were merged by a dichroic mirror and focused by an achromatic lens ($f = 250$ nm) into a pulsed Kr jet. The fundamental beams, four-wave sum frequency and difference frequency beams were separated by a toroidal grating that was also used to focus the XUV laser [31]. The probe UV laser ionizing the photofragments was from the doubling of the third dye laser pumped by the second Nd:YAG laser. The delay-time scan of the probe laser pulse relative to the XUV laser pulse was controlled by a personal computer and realized by a digital delay controller (DG 535). The pulsed HD beam was produced by a pulsed valve (General Valve Corp.). The stagnation pressure of the HD gas was about 1500 Torr and the purity of the HD sample was better than 98%.

The branching ratios [H($2s$)]/[H($2s$) + H($2p$)] and [D($2s$)]/[D($2s$) + D($2p$)], designated as α_H and α_D, respectively, were measured using the so-called delay-time-curve method. Note that the symbol [x] represents the population of the X state in this paper. In this method, the H($2s$, $2p$) or D($2s$, $2p$) signals were recorded as a function of the time delay between the XUV pump laser and the UV probe laser pulses under the field-free condition. The extraction electric pulse voltage (2 kV) for the H^+ and D^+ cations was applied about 200 ns after the XUV laser pulse. The sensitivities of the microchannel plate detector to the H^+ and D^+ ions were assumed to be equal, as previously illustrated [36]. The branching ratios α_H and α_D were determined using a simulation considering the lifetime of the $2s$ (0.14 s) and $2p$ (1.6 ns) states and the temporal pulse widths of the pump and probe lasers (∼6 ns). The probe laser was focused with an $f = 300$ mm lens. Because of the large ionization cross sections, the ionization rate should be much larger than the decay rate of the $2p$ state [25].

The relative ratios [H($2s$, $2p$)]/[D($2s$, $2p$)] between the H($2s$, $2p$) + D($1s$) and the D($2s$, $2p$) + H($1s$) channels were determined by comparing the maximum of the two delay-time curves recorded simultaneously. The four-channel branching ratios can be calculated easily using the measured values of α_H, α_D, and [H($2s$, $2p$)]/[D($2s$, $2p$)]. We denote the normalized branching ratios for the following four channels as x_1, x_2, x_3, and x_4, respectively:

$$\mathrm{HD} + h\nu \rightarrow \mathrm{H}(2s) + \mathrm{D}(1s), \quad (1)$$

$$\mathrm{HD} + h\nu \rightarrow \mathrm{H}(2p) + \mathrm{D}(1s), \quad (2)$$

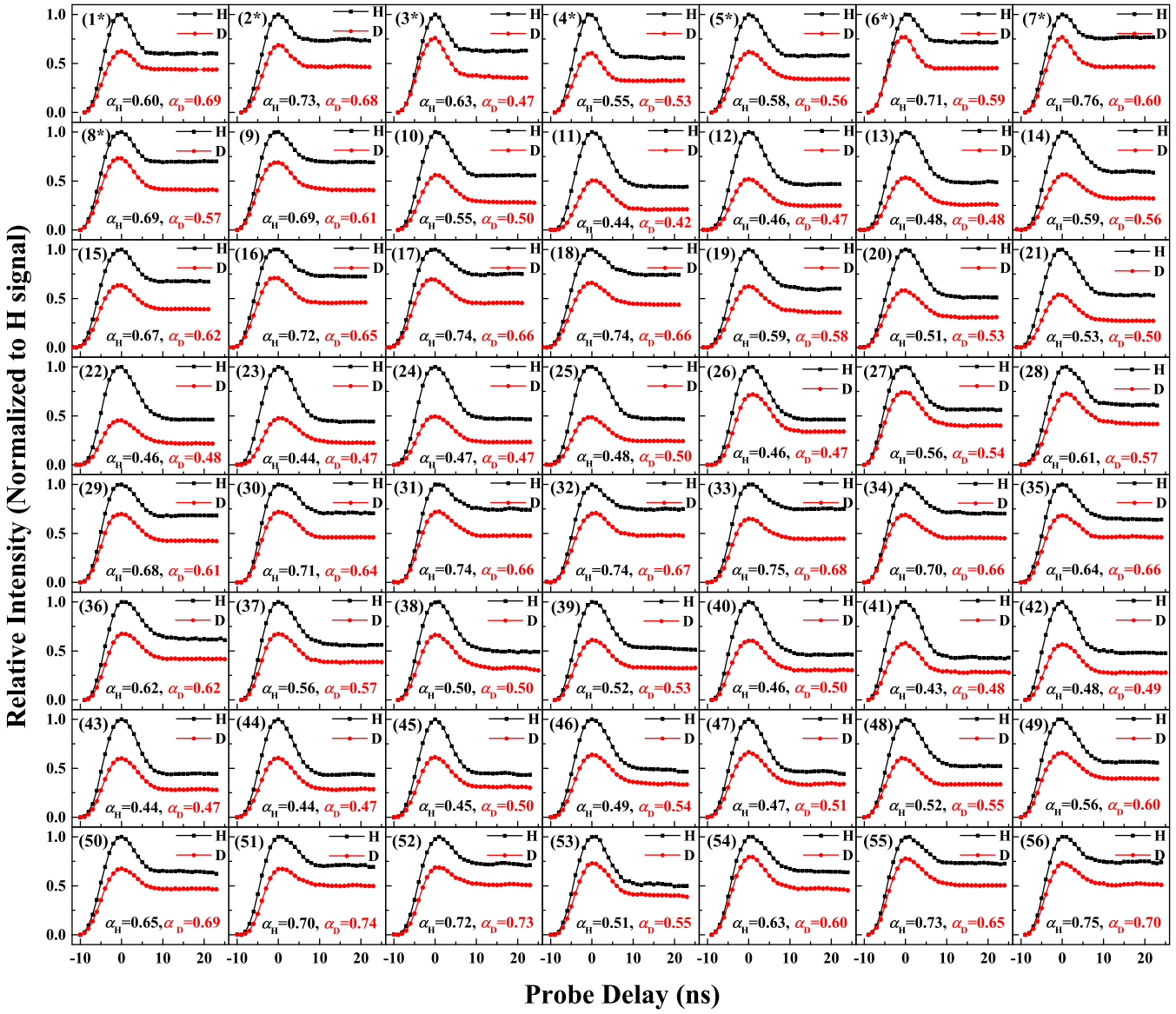

FIG. 2. Delay-time curves of the H($2s$, $2p$) and D($2s$, $2p$) fragments from the direct photodissociation of HD. The signal intensities are normalized to the maximum of H($2s$, $2p$). The relative intensities [D($2s$, $2p$)]/[H($2s$, $2p$)] are obtained from the maximum of D($2s$, $2p$) signals in the figure. The corresponding excitation energies can be found in the Supplemental Material using the panel numbers [37].

$$\mathrm{HD} + h\nu \rightarrow \mathrm{D}(2s) + \mathrm{H}(1s), \tag{3}$$

$$\mathrm{HD} + h\nu \rightarrow \mathrm{D}(2p) + \mathrm{H}(1s). \tag{4}$$

We have the relationships

$$\frac{x_1}{x_1 + x_2} = \frac{[\mathrm{H}(2s)]}{[\mathrm{H}(2s) + \mathrm{H}(2p)]} = \alpha_\mathrm{H}, \tag{5}$$

$$\frac{x_3}{x_3 + x_4} = \frac{[\mathrm{D}(2s)]}{[\mathrm{D}(2s) + \mathrm{D}(2p)]} = \alpha_\mathrm{D}, \tag{6}$$

$$\frac{x_1 + x_2}{x_3 + x_4} = \frac{[\mathrm{H}(2s, 2p)]}{[\mathrm{D}(2s, 2p)]}, \tag{7}$$

$$x_1 + x_2 + x_3 + x_4 = 1. \tag{8}$$

III. RESULTS AND DISCUSSION

Figure 2 shows all the measured delay-time curves for the branching ratios α_H and α_D. Figure 3 shows two expanded figures for them. The numerical values can be found in the figure and the Supplemental Material [37].

Our supersonic HD beam had a rotational state distribution, which was approximately 0.80:0.16:0.04 for the $J'' = 0$, 1, 2 states, respectively, estimated from the $R(0)$, $R(1)$, and $R(2)$ transition intensities of $4p\sigma\ ^1\Sigma_u^+ \leftarrow X\ ^1\Sigma_g^+$ [25]. The contributions from the rotational states $J'' \geqslant 1$ to the branching ratios α_H and α_D of the first eight points in Fig. 2 can be excluded based on the velocity map images measured under the electric-field and field-free conditions, respectively. The detailed procedure and the measured velocity map images can be found in the Supplemental Material [37]. Because of the limited resolution of the fragment translational energies, we

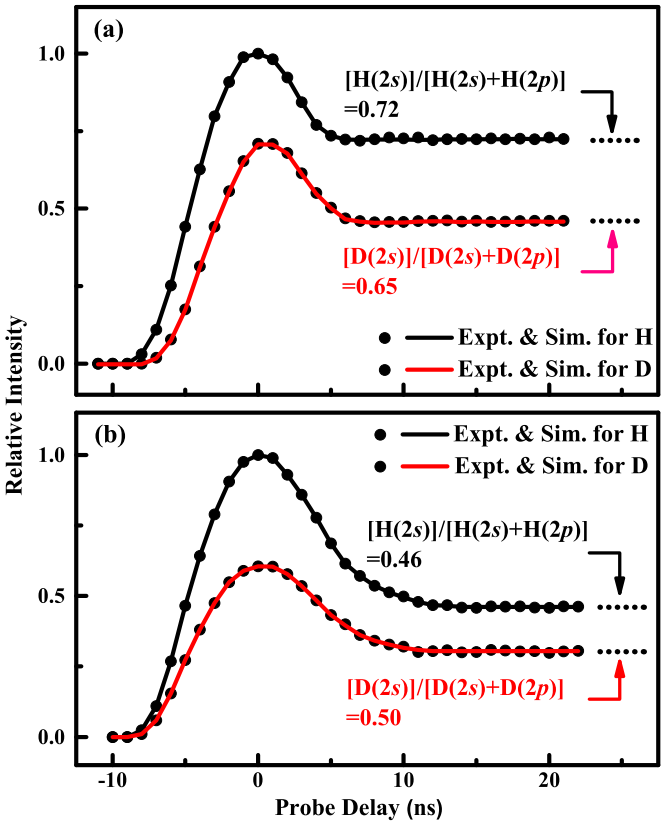

FIG. 3. Two expanded curves from Fig. 1. (a) Panel (16) of Fig. 1 with excitation energy 119 600.1 cm^{-1}. (b) Panel (40) of Fig. 1 with excitation energy 120 960.1 cm^{-1}. The dots show the experimental data and the solid curves represent the simulations.

could not obtain the branching ratios of the pure $J'' = 0$ state for the latter points. However, the measured branching ratios could be regarded as from the $J'' = 0$ state because (a) most of the rotational states are in the $J'' = 0$ state (~80%) and (b) the branching ratios α_H and α_D are mainly determined by the available energies of the fragments [11]. For the ninth point in Fig. 2 (the minimum excitation energy without the correction of the branching ratio from the $J'' \geqslant 1$ states), the fragments have an available energy of 490 cm^{-1} that is much larger than the rotational energy of the $J'' = 1$ state (~89 cm^{-1}).

Figures 4(a1) and 4(a2) show the normalized four-channel branching ratios. Figures 4(b1) and 4(b2) show the relative ratios of $[H(2s)]/[H(2s) + D(2s)]$ and $[H(2p)]/[H(2p) + D(2p)]$, and $[H(2s, 2p)]/[D(2s, 2p)]$, respectively. It can be seen in Figs. 4(a1) and 4(a2) that the branching ratios of the H(2s), D(2s), H(2p), and D(2p) fragments all oscillate with the excitation energies. Furthermore, the branching ratios of the H(2s) fragments oscillate with the same phase as that of the D(2s) fragments, and the branching ratios of the H(2p) fragments also oscillate with a phase similar to that of the D(2p) fragments. By examining Figs. 4(a1) and 4(a2) carefully, it is also found that the oscillation of the H(2s) fragments is out of phase with that of the H(2p) fragment, as are the phases between the D(2s) and D(2p) fragments. For H_2 and D_2, the oscillations of the H(2s) and D(2s) fragments are also out of phase with the H(2p) and D(2p) fragments, respectively [11,15]. As can be seen in Fig. 4(b1), the ratios $[H(2s)]/[H(2s) + D(2s)]$ and $[H(2p)]/[H(2p) + D(2p)]$ are ~0.60. In the following, we assume that $[2s] = [H(2s) + D(2s)]$, $[2p] = [H(2p) + D(2p)]$, and $[2s + 2p] = [H(2p) + D(2p) + H(2s) + D(2s)]$. A list of branching ratios can be found in Tables S1 and S2 in [37].

The yield spectra of the H(2s, 2p) and D(2s, 2p) fragments reported in our previous work are also shown at the bottom of Figs. 4(a1) and 4(a2), respectively [25]. The sharp peaks are from the predissociation of HD, and their linewidths are usually less than 1 cm^{-1} in the energy range we studied (except for several weak peaks with linewidths ranging from 3 to 7 cm^{-1}) [25]. We have taken care to avoid measuring the branching ratios in the neighborhood of the peaks so that the measured ones were from the dissociation of the continuum states. In the predissociation of HD, there are generally more H(2s) or H(2p) fragments produced than D(2s) or D(2p) fragments, which is also true in the direct dissociation of HD. However, for the predissociation of HD, the values of $[H(2s, 2p)]/[D(2s, 2p)]$ range from 1.9 to 4.0, depending on the predissociated states, which are different from that of ~1.6 for the direct dissociation of HD [see Fig. 4(b2)]. The reason for the difference should be studied in future theoretical studies.

Figures 5(a), 5(b), and 5(c) show the relative branching ratios $[H(2s)]/[H(2s) + H(2p)]$, $[D(2s)]/[D(2s) + D(2p)]$, and $[2s]/[2s + 2p]$, respectively, as functions of the wave vector k of the photofragments, $k = \sqrt{2\mu E_t}/\hbar$, where E_t is the translational energy of the fragments in the center-of-mass coordinate, μ is the reduced mass of HD, and $\hbar$ is the reduced Planck constant. All of them oscillate as functions of the wave vector k and are similar to cosine functions.

Based on the above observations, we propose the following dissociation mechanism. In the Franck-Condon region, the photodissociation dynamics of HD is similar to those of H_2 and D_2, i.e., only the u-symmetry states are excited. The branching ratios $[2s]/[2s + 2p]$ should be controlled by the interferences between the $3p\sigma B'\,^1\Sigma_u^+$ and $2p\sigma B\,^1\Sigma_u^+$ states, similar to those of H_2 and D_2, but with different reduced masses. This mechanism is supported by experimental results shown in Fig. 5(c). Near the dissociation limits, there are population redistributions of the 2s and 2p states from the H atom to the D atom and vice versa due to the mixing of g-u states. The g-u pairwise interaction between the $3p\sigma B'\,^1\Sigma_u^+$ and $GK\,^1\Sigma_g^+$ states controls the channel distributions between D(2s) + H(1s) and H(2s) + D(1s), while the pairwise interactions between the $EF\,^1\Sigma_g^+$ and $2p\sigma B\,^1\Sigma_u^+$ states and between the $2p\pi C\,^1\Pi_u$ and $II'\,^1\Pi_g$ states control the ratios between H(2p) + D(1s) and D(2p) + H(1s) [20–22].

Note that the corrected adiabatic electronic wave function near the dissociation limits can be approximated by

$$\Psi^{(\pm)} = \frac{1}{\sqrt{2}}[\phi_g(R, r) \pm \phi_u(R, r)], \tag{9}$$

where $\phi_g(R, r)$ and $\phi_u(R, r)$ are the electronic wave functions of the Born-Oppenheimer approximation. If the fragment kinetic energies are much larger than 22 cm^{-1} [the energy space between the channels D(2l) + H(1s) and H(2l) + D(1s)], 50% of the populated u-symmetry states in the Franck-Condon region should go to the upper and lower adiabatic

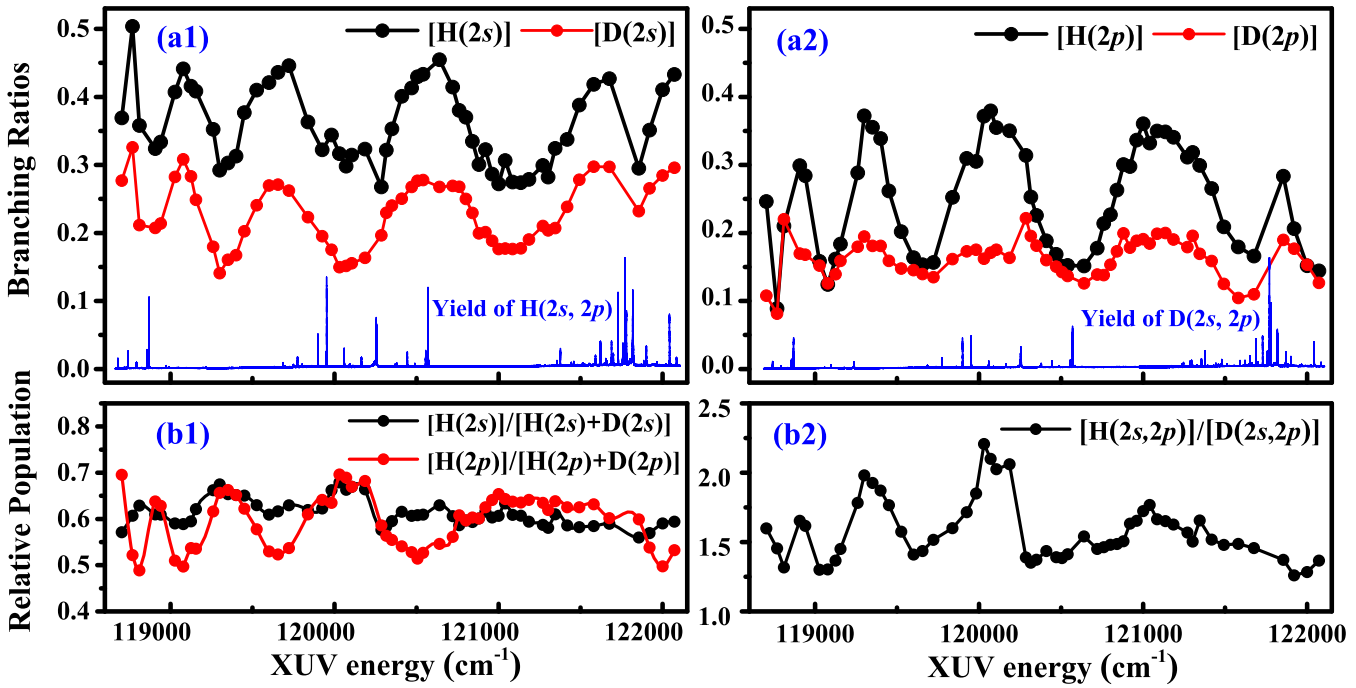

FIG. 4. Branching ratios and relative populations in the direct dissociation of HD + $h\nu \rightarrow$ H(2s, 2p) + D(1s) and D(2s, 2p) + H(1s): (a1) branching ratios of H(2s) and D(2s), (a2) branching ratios of H(2p) and D(2p), (b1) [H(2s)][/D(2s) + H(2s)] and [H(2p)]/[H(2p) + D(2p)], and (b2) [H(2s, 2p)]/[D(2s, 2p)]. The dots show the experimental data and the solid lines are to guide the eye. The curves shown at the bottom of (a1) and of (a2) are the H(2s, 2p) and D(2s, 2p) fragment yield spectra, respectively, in which the peaks are from the predissociation of HD [25].

states, respectively, which is called the diabatic approximation. In the present case, the PECs calculated using the Born-Oppenheimer approximation without account of the atomic masses may be regarded as diabatic PECs, although it is usually called the adiabatic approximation [1,22].

As mentioned above, the ratio [H(2s)]/[D(2s) + H(2s)] is ~0.6, which indicate that 60% of the $3p\sigma B'\,^1\Sigma_u^+$ states correlated with D(2s) + H(1s) have transferred to the $EF\,^1\Sigma_g^+$ states correlated with H(2s) + D(1s) near the dissociation limits. On the other hand, we also expect that 40% of the $2p\sigma B\,^1\Sigma_u^+$ states correlated with H(2p) + D(1s) are transferred to the $GK\,^1\Sigma_g^+$ state correlated with D(2p) + H(1s).

For the relative channel branching ratios between the channels H(2s) + D(1s) and H(2p) + D(1s) we have

$$\frac{[\mathrm{H}(2s)]}{[\mathrm{H}(2s)]+[\mathrm{H}(2p)]}=\frac{k_1[2s]}{k_1[2s]+k_2[2p]}, \tag{10}$$

where $k_1 = [\mathrm{H}(2s)]/[2s]$ and $k_2 = [\mathrm{H}(2p)]/[2p]$. For the diabatic model discussed above, we should have $k_1 = k_2 = 0.5$, and hence

$$\frac{[\mathrm{H}(2s)]}{[\mathrm{H}(2s)]+[\mathrm{H}(2p)]}=\frac{[2s]}{[2s+2p]}. \tag{11}$$

For the D fragments, we have a similar equation. Therefore, we have

$$\frac{[\mathrm{H}(2s)]}{[\mathrm{H}(2s)]+[\mathrm{H}(2p)]}=\frac{[\mathrm{D}(2s)]}{[\mathrm{D}(2s)]+[\mathrm{D}(2p)]}=\frac{[2s]}{[2s+2p]}. \tag{12}$$

Equation (12) illustrates that the relative branching ratios of [H(2s)]/[H(2s) + H(2p)], [D(2s)]/[D(2s) + D(2p)], and [2s]/[2s + 2p] should be similar in the direct dissociation of HD if the diabatic approximation is valid near the dissociation limits. The above supposition is supported by Fig. 4(b1). It is therefore concluded that there is an almost complete mixing of the g-u states near the dissociation limits. Note that the experimental results show $k_1 \approx k_2 \approx 0.60$.

For the direct dissociation of H_2 or D_2, the branching ratio of [H(2s)]/[H(2s) + H(2p)] or [D(2s)]/[D(2s) + D(2p)] can be approximately described by [11,15]

$$\frac{\tilde{\sigma}_{2s}}{\tilde{\sigma}_{2s}+\tilde{\sigma}_{2p}}=\tilde{r}_A+\tilde{r}_B\cos\left(\delta_{l(2s)}-\delta_{l(2p)}\right), \tag{13}$$

where $\delta_{l(2s)}$ and $\delta_{l(2p)}$ are the phase shifts of the lth wave relative to the free spherical waves due to the potential energy curves of the $3p\sigma B'\,^1\Sigma_u^+$ and $2p\sigma B\,^1\Sigma_u^+$ states, respectively. In addition, $\tilde{r}_A$ is the branching ratio when the two scattering functions are out of phase ($\pi/2$) and $\tilde{r}_B$ may be regarded as the modulation depth of the branching ratio. As shown in Eq. (12), the branching ratios [H(2s)]/[H(2s) + H(2p)], [D(2s)]/[D(2s) + D(2p)], and [2s]/[2s + 2p] of the dissociation of HD should be described by Eq. (13).

As we have done previously [15], we used an effective potential model to describe the phase shift, which is similar to multichannel quantum defect theory [13,14]. In this model, the diatomic interaction potentials are assumed to be spherical potential wells, characterized by depth $-\tilde{U}$ and width $\tilde{a}$.

For the photoexcitation starting from $J'' = 0$, only the final state of $J'' = 1$ is possible. We assume that the coupling between the electronic angular momentum and the nuclear

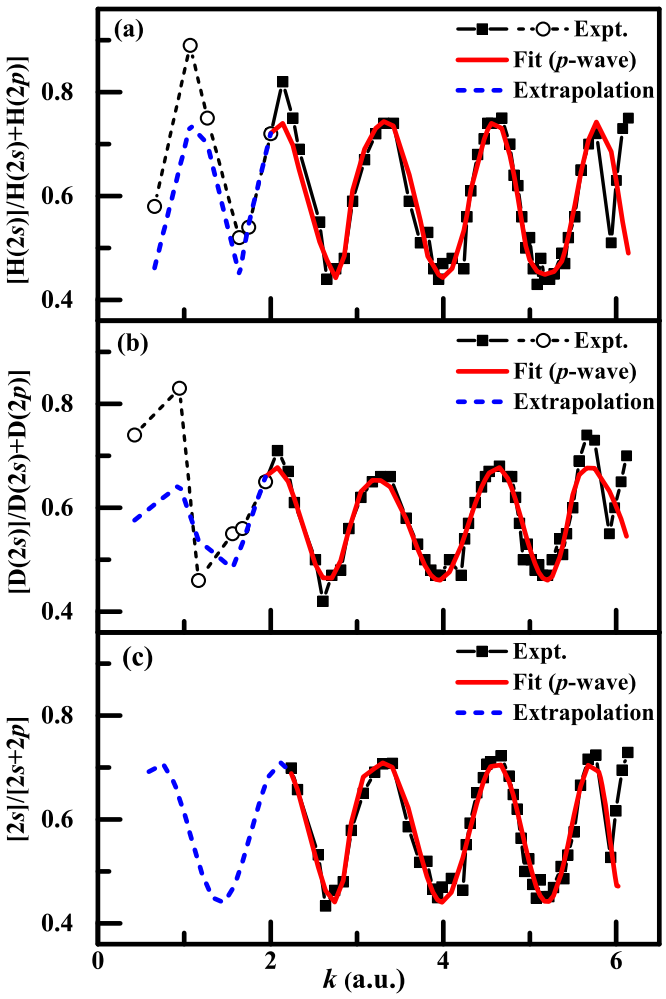

FIG. 5. Relative channel branching ratios as functions of the wave vector k of the photofragments (in a.u.): (a) $[H(2s)]/[H(2s)+H(2p)]$, (b) $[D(2s)]/[(2s)+D(2p)]$, and (c) $[2s]/[2s+2p]$. In (c), k values are assumed to be the same as those of the lower-energy threshold channel $HD \rightarrow H(2s)+D(1s)$. The closed squares and open circles show the experimental data and the solid curves are the fits using Eqs. (13) and (15). The first six points (open circles) near the threshold are not included in the fits.

rotational angular momentum is weak, and therefore only a p wave ($l=1$) is possible. The p-wave phase shift can be approximated by [15]

$$\delta_1 \approx -k\tilde{a} + \cot^{-1}\left(\frac{k\cot\tau\tilde{a}}{\tau}\right) \quad \text{for } \tau \gg k,\ \tilde{a}k \gg 1, \quad (14)$$

where $\tau = \sqrt{2\mu(E_t+\tilde{U}_0)}/\hbar$. The phase difference between the two channels is thus determined by

$$\delta_{1(2p)} - \delta_{1(2s)} \approx -k(\tilde{a}_{2p}-\tilde{a}_{2s}) + \cot^{-1}\left(\frac{k\cot\tau_{2p}\tilde{a}_{2p}}{\tau_{2p}}\right) - \cot^{-1}\left(\frac{k\cot\tau_{2s}\tilde{a}_{2s}}{\tau_{2s}}\right). \quad (15)$$

In this equation, the first term is dominant, and thus the phase difference is determined mainly by the wave vector k. As can be seen from Eqs. (13) and (15), the branching ratio is a cosine function of the wave vector of the photofragments [15].

Using Eqs. (13) and (15), we fitted the measured branching ratios employing the nonlinear least-squares method. The results are shown in Fig. 5. For Figs. 5(a) and 5(b), the branching ratios in the lower six points of k values were not included in the fits, yet the extensions of the fits to the low-k values are in agreement with the experimental data. The $\tilde{U}$ and $\tilde{a}$ values of the two spherical potential wells were obtained from the fits and are listed in Table I, along with the parameters $\tilde{r}_A$ and $\tilde{r}_B$ in Eq. (13). From Table I it is known that all the parameters, including $\tilde{r}_A$, $\tilde{r}_B$ and width and depth of the effective potential wells, are similar from fitting the branching ratios $[H(2s)]/[H(2s)+H(2p)]$, $[D(2s)]/[D(2s)+D(2p)]$, and $[2s]/[2s+2p]$. The results are in agreement with Eq. (12). The difference of the $\tilde{r}_A$ and $\tilde{r}_B$ values between HD and D_2 may be due to the reduced masses of the two isotopologues.

To compare the effective spherical potential wells with those of the *ab initio* PECs, the effective width $\tilde{a}$ and depth $\tilde{U}$ for a theoretical PEC $[U(r)]$ are assumed to be

$$\tilde{a} = \frac{\int_0^\infty r\,U(r)r^2dr}{\int_0^\infty U(r)r^2dr}, \qquad -\tilde{U} = \frac{\int_0^\infty 4\pi U(r)r^2dr}{\frac{4}{3}\pi\tilde{a}^3}. \quad (16)$$

TABLE I. Parameters obtained from fitting the channel branching ratios [see Eqs. (13), (15), and (16) for the definitions of the parameters. Here $\tilde{r}_A$ and $\tilde{r}_B$ denote the cosine oscillations of the branching ratios and $\tilde{a}$ and $-\tilde{U}$ represent the widths and depths of the effective potential wells, respectively, of the $2p\sigma\,B\,^1\Sigma_u^+$ and $3p\sigma\,B'\,^1\Sigma_u^+$ states.

	HD					
Method	$\tilde{a}$ $(2p\sigma)$ (a.u.)	$-\tilde{U}$ $(2p\sigma)$ (10^3 cm^{-1})	$\tilde{a}$ $(3p\sigma)$ (a.u.)	$-\tilde{U}$ $(3p\sigma)$ (10^3 cm^{-1})	$\tilde{r}_A$	$\tilde{r}_B$
PEC[a]	6.46	30.6	1.81	12.0		
$[H(2s)]/[H(2s)+H(2p)]$[b]	6.5 ± 0.4	31 ± 4	1.7 ± 0.4	11 ± 3	0.59 ± 0.01	0.16 ± 0.01
$[D(2s)]/[D(2s)+D(2p)]$[b]	6.4 ± 0.4	32 ± 5	1.6 ± 0.4	13 ± 4	0.57 ± 0.01	0.10 ± 0.01
$[2s]/[2s+2p]$[b]	6.5 ± 0.4	34 ± 6	1.7 ± 0.4	12 ± 3	0.58 ± 0.01	0.14 ± 0.01
			D_2			
Expt.[c]	6.4 ± 0.4	33 ± 5	1.6 ± 0.4	12 ± 4	0.76 ± 0.01	0.11 ± 0.01

[a]Calculated from the *ab initio* PECs using Eq. (16) [15].
[b]From a fit of the corresponding relative branching ratios.
[c]From a fit of the branching ratios $[D(2s)]/[D(2s)+D(2p)]$ in the photodissociation of the D_2 molecule [15].

Note that the starting point of the effective potential $r = 0$ in this equation corresponds to an internuclear distance of $R = 1.0$ a.u., where the potential is very large [15]. The results are listed in Table I.

It can be seen in Table I that the effective parameters of the potential wells determined from the fits of the experimental data of HD are in good agreement with those resulting from the *ab initio* PECs [15]. This agreement demonstrates that oscillations of the branching ratios can be explained by the interferences of the two pathways between the $3p\sigma B'\,^1\Sigma_u^+$ and $2p\sigma B\,^1\Sigma_u^+$ states, as indicated previously [11,12,15], and the *g-u* state mixings near the dissociation limits.

IV. SUMMARY

We have measured the channel branching ratios of $H(2s) + D(1s)$, $H(2p) + D(1s)$, $D(2s) + H(1s)$, and $D(2p) + H(1s)$ in the direct dissociation of HD, with all of them oscillating as functions of wave vectors of the photofragments. The relative channel branching ratios $[H(2s)]/[H(2s) + H(2p)]$, $[D(2s)]/[D(2s) + D(2p)]$, and $[2s]/[2s + 2p]$ oscillate with nearly the same phases and similar amplitudes. The results can be explained by the following mechanisms: (a) The photodissociation follows the usual Born-Oppenheimer approximation in the Franck-Condon region and (b) near the dissociation limits, the *g-u* pair states are mixed almost completely, which controls the relative ratios between the $H(2s)$ and $D(2s)$ fragments and between the $H(2p)$ and $D(2p)$ fragments. The results presented in this work provide insight into the *g-u* state mixing and in general the adiabatic state mixing near the dissociation limits in the photodissociation of molecules.

ACKNOWLEDGMENTS

This work was funded by Projects No. 21833003 and No. 21773134 supported by the National Natural Science Foundation of China and National Key R&D program of China (Grant No. 2018YFA0306504).

[1] H. Lefebvre-Brion and R. W. Field, *The Spectra and Dynamics of Diatomic Molecules* (Academic Press, New York, 2004).

[2] A. N. Heays, A. D. Bosman, and E. F. van Dishoeck, Photodissociation and photoionization of atoms and molecules of astrophysical interest, Astron. Astrophys. **602**, A105 (2017).

[3] H. Gao and C. Y. Ng, Quantum state-to-state vacuum ultraviolet photodissociation dynamics of small molecules, Chin. J. Chem. Phys. **32**, 23 (2019).

[4] C. Cohen-Tannoudji and D. Guery-Odelin, *Advance in Atomic Physics: An Overview* (World Scientific, Hackensack, 2011).

[5] R. Krems, B. Friedrich, and W. Stwalley, *Cold Molecules: Theory, Experiment, Applications* (Taylor & Francis, London, 2010).

[6] N. Hölsch, M. Beyer, E. J. Salumbides, K. S. E. Eikema, W. Ubachs, C. Jungen, and F. Merkt, Benchmarking Theory with an Improved Measurement of the Ionization and Dissociation Energies of H_2, Phys. Rev. Lett. **122**, 103002 (2019).

[7] M. Puchalski, J. Komasa, P. Czachorowski, and K. Pachucki, Nonadiabatic QED Correction to the Dissociation Energy of the Hydrogen Molecule, Phys. Rev. Lett. **122**, 103003 (2019).

[8] A. Monfils, The absorption spectra of the molecules H_2, HD, and D_2: Part VI. Rotational analysis of the B', B'', D, D', and D'' states, J. Mol. Spectrosc. **15**, 265 (1965).

[9] M. Rothschild, H. Egger, R. T. Hawkins, J. Bokor, H. Pummer, and C. K. Rhodes, High-resolution spectroscopy of molecular hydrogen in the extreme ultraviolet region, Phys. Rev. A **23**, 206 (1981).

[10] E. E. Eyler and N. Melikechi, Near-threshold continuum structure and dissociation energies of H_2, HD, and D_2, Phys. Rev. A **48**, R18 (1993).

[11] J. A. Beswick and M. Glass-Maujean, Interference effects on the $H(2p)$ to $H(2s)$ branching ratio in the photodissociation of hydrogen and deuterium, Phys. Rev. A **35**, 3339 (1987).

[12] M. Glass-Maujean, H. Frohlich, and J. A. Beswick, Experimental Evidence of an Interference between Photodissociation Continua, Phys. Rev. Lett. **61**, 157 (1988).

[13] H. Gao, C. Jungen, and C. H. Greene, Predissociation of H_2 in the $3p\pi D\,^1\Pi_u^+$ state, Phys. Rev. A **47**, 4877 (1993).

[14] J. Z. Mezei, I. F. Schneider, M. Glass-Maujean, and C. Jungen, Resonances in photoabsorption: Predissociation line shapes in the $3p\pi D\,^1\Pi_u^+ \leftarrow X\,^1\Sigma_g^+$ system in H_2, J. Chem. Phys. **141**, 064305 (2014).

[15] J. Wang, Q. Meng, and Y. Mo, Oscillation of Branching Ratios between the $D(2s) + D(1s)$ and the $D(2p) + D(1s)$ Channels in Direct Photodissociation of D_2, Phys. Rev. Lett. **119**, 053002 (2017).

[16] R. Liyanage, Y. A. Yang, S. Hashimoto, R. J. Gordon, and R. W. Field, Electronic control of the spin-orbit branching ratio in the photodissociation of HCl, J. Chem. Phys. **103**, 6811 (1995).

[17] M. H. Alexander, X. Li, R. Liyanage, and R. J. Gordon, Spin-orbit branching in the predissociation of the $C\,^1\Pi$ state of HCl and DCl: A manifestation of quantum interference, Chem. Phys. **231**, 331 (1998).

[18] J. Wang and Y. Mo, Predissociation dynamics of $D_2 + h\nu \rightarrow D(1s_{1/2}) + D(2p_{1/2,3/2}, 2s_{1/2})$ revealed by the spin-orbit state resolved fragment branching ratios and angular distributions, J. Chem. Phys. **150**, 144306 (2019).

[19] J. Durup, On isotope effects in the predissociations of HD, J. Phys. (Paris) **39**, 941 (1978).

[20] A. de Lange, E. Reinhold, W. Hogervorst, and W. Ubachs, Gerade/ungerade symmetry-breaking in HD at the $n = 2$ dissociation limit, Can. J. Phys. **78**, 567 (2000).

[21] T. G. P. Pielage, A. de Lange, F. Brandi, and W. Ubachs, Bound energy levels at the $n = 2$ dissociation threshold in HD, Chem. Phys. Lett. **366**, 583 (2002).

[22] A. de Lange, E. Reinhold, and W. Ubachs, Phenomena of *g-u* symmetry breakdown in HD, Int. Rev. Phys. Chem. **21**, 257 (2002).

[23] T. P. Grozdanov and R. McCarroll, Gerade-ungerade symmetry in HD: Bound states supported by the $I'\,^1\Pi_g$ outer potential well, J. Chem. Phys. **128**, 114317 (2008).

[24] T. P. Grozdanov and R. McCarroll, Gerade-ungerade symmetry breaking in bound states localized in the $II'\,^1\Pi_g$ outer potential well of HD, Phys. Scr. **80**, 048123 (2009).

[25] J. Wang and Y. Mo, Isotope effect and gerade versus ungerade symmetry in HD predissociation revealed by the H($2s$), H($2p$), D($2s$), and D($2p$) fragments, Phys. Rev. A **98**, 062509 (2018).

[26] I. Dabrowski and G. Herzberg, The absorption and emission spectra of HD in the vacuum ultraviolet, Can. J. Phys. **54**, 525 (1976).

[27] K. Tsukiyama and Y. Ogi, The fluorescence lifetime of the *gerade* states of HD near the second dissociation limit, J. Mol. Spectrosc. **312**, 87 (2015).

[28] G. D. Dickenson and W. Ubachs, The $D\,^1\Pi_u$ state of HD and the mass scaling relation of its predissociation widths, J. Phys. B **45**, 145101 (2012).

[29] D. Sprecher and F. Merkt, Observation of *g*/*u* mixing in the high-n Rydberg states of HD, J. Chem. Phys. **140**, 124313 (2014).

[30] T. I. Ivanov, G. D. Dickenson, M. Roudjane, N. de Oliveria, D. Joyeux, L. Nahon, W.-Ü. L. Tchang-Brillet, and W. Ubachs, Fourier-transform spectroscopy of HD in the vacuum ultraviolet at $\lambda = 87-112$ nm, Mol. Phys. **108**, 771 (2010).

[31] Y. Mo, J. Yang, and G. Chen, Zero kinetic energy photoelectron study of $SO_2^+(X\,^2A_1)$ using coherent extreme ultraviolet radiation, J. Chem. Phys. **120**, 1263 (2004).

[32] Q. Meng and Y. Mo, Predissociation dynamics in the $3p\pi D\,^1\Pi_u^{\pm}(\upsilon = 3)$ and $4p\sigma B''^1\Sigma_u^+(\upsilon = 1)$ states of H_2 revealed by product branching ratios and fragment angular distributions, J. Chem. Phys. **144**, 154305 (2016).

[33] Q. Meng, J. Wang, and Y. Mo, Angle-resolved Beutler-Fano profile and dynamics for the predissociation of H_2, Phys. Rev. A **93**, 050501(R) (2016).

[34] J. Wang, Q. Meng, and Y. Mo, Electronic and Tunneling predissociations in the $2p\pi C^1\Pi_u{}^{\pm}(\upsilon = 19)$ and $3p\pi D^1\Pi_u{}^{\pm}(\upsilon = 4, 5)$ states of D_2 studied by a combination of XUV laser and velocity map imaging, J. Phys. Chem. A **121**, 5785 (2017).

[35] L. Wang and Y. Mo, photodissociation of HCl in the photon energy range 14.6–15.0 eV: Channel resolved branching ratios and fragment angular distributions, J. Chem. Phys. **152**, 014309 (2020).

[36] B. Brehm, J. Grosser, T. Ruscheinski, and M. Zimmer, Absolute detection efficiencies of a microchannel plate detector for ions, Meas. Sci. Technol. **6**, 953 (1995).

[37] See Supplemental Material at http://link.aps.org/supplemental/10.1103/PhysRevA.101.053418 for additional details.